Entanglement complexity of the Rokhsar-Kivelson-sign wavefunctions

Stefano Piemontese,[1,*] Tommaso Roscilde,[2] and Alioscia Hamma[1,3,4]
[1]*Physics Department, University of Massachusetts Boston, Boston, Massachusetts 02125, USA*
[2]*Univ Lyon, Ens de Lyon, CNRS, Laboratoire de Physique, F-69342 Lyon, France*
[3]*Dipartimento di Fisica "Ettore Pancini," Università degli Studi di Napoli Federico II, Via Cintia, 80126 Napoli, Italy*
[4]*INFN, Sezione di Napoli, 80126 Napoli, Italy*

(Received 18 November 2022; revised 27 February 2023; accepted 28 February 2023; published 13 April 2023)

Entanglement comes in different forms, some more complex than others. In this paper we study the transitions of entanglement complexity in an exemplary family of states—the Rokhsar-Kivelson-sign wavefunctions—whose degree of entanglement is controlled by a single parameter. This family of states is known to feature a transition between a phase exhibiting volume-law scaling of entanglement entropy and a phase with subextensive scaling of entanglement, reminiscent of the many-body-localization transition of disordered quantum Hamiltonians. We study the singularities of the Rokhsar-Kivelson-sign wavefunctions and their entanglement complexity across the transition using several tools from quantum information theory: fidelity metric, entanglement spectrum statistics, entanglement entropy fluctuations, stabilizer Rényi entropy, and the performance of a disentangling algorithm. Across the whole volume-law phase the states feature universal entanglement spectrum statistics. Yet a "superuniversal" regime appears for small values of the control parameter in which all metrics become independent of the parameter itself, the entanglement entropy as well as the stabilizer Rényi entropy appear to approach their theoretical maximum, the entanglement fluctuations scale to zero as in output states of random universal circuits, and the disentangling algorithm has essentially null efficiency. All these indicators consistently reveal a complex pattern of entanglement. In the sub-volume-law phase, on the other hand, the entanglement spectrum statistics is no longer universal, entanglement fluctuations are larger and exhibiting a nonuniversal scaling, and the efficiency of the disentangling algorithm becomes finite. Our results, based on model wavefunctions, suggest that a similar combination of entanglement scaling properties and of entanglement complexity features may be found in high-energy Hamiltonian eigenstates—a very strong candidate being offered by the many-body localization transition of disordered lattice-spin models.

DOI: 10.1103/PhysRevB.107.134202

I. INTRODUCTION

A. Entanglement and its complexity

Quantum entanglement is often considered as being the defining characteristic of quantum mechanics and it is a fundamental notion for some of the behavior that is impossible for local classical physics, such as Bell nonlocality [1,2]. In the context of quantum information, quantum entanglement represents the resource behind the computational speed-up offered by quantum algorithms and the central ingredient enabling protocols such as quantum teleportation [3–6].

Since entanglement represents a fundamental form of quantum correlations between different local parts of a system, the question of its physical significance in quantum many-body systems has surged to great importance in the past two decades [7,8]. Quantum many-body systems are typically governed by Hamiltonians featuring local interactions and this locality is responsible for the spatial decay of correlations in the ground state, as well as for the area-law scaling of the entanglement entropy of a subsystem [8–10] corresponding, e.g., to the von Neumann entropy of the subsystem density matrix. Entanglement has provided fundamental insights in the study of quantum many-body phenomena, such as quantum phase transitions (QPTs) [11–17], exotic phases of matter featuring topological order [18–22], and quantum many-body localization [23–29].

More recently, it has been recognized that entanglement properties of wavefunctions go beyond a single quantity such as the entanglement entropy of a subsystem. Beyond the notion of bipartite and multipartite entanglement [30–32], it has also been recognized that entanglement can be more or less *complex* [33–35], in relationship with the resources needed to produce it. The complexity of entanglement can be associated with an ensemble of properties that appear to be concomitant, namely the following.

(i) The emergence of a universal entanglement spectrum statistics, namely a universal distribution for the gaps of the entanglement spectrum, compatible with the Wigner-Dyson distribution.

(ii) The fact that it can only be produced by resources that go beyond those required to produce stabilizer states, namely quantum gates that fall outside of the Clifford group and are sufficient for universal quantum computation [36,37], which are responsible for any computational advantage in quantum information processing [38]. This notion of

*s.piemontese001@umb.edu

"nonstabilizerness" has also been commonly referred to as *magic* in the recent literature [39–43].

(iii) The scaling of entanglement fluctuations corresponding to those of random states in the Hilbert space, as well as of output states of random circuits using universal resources [44,45].

(iv) The failure of a disentangling algorithm based on Metropolis sampling of Clifford random circuits [33,34,45], whereas states with simple patterns of entanglement can be efficiently disentangled by such annealing methods.

Interestingly, the presence of magic is in principle independent of the scaling of the entanglement entropy. Indeed there are states which are not entangled and which possess magic—e.g., states produced by single-qubit gates which are out of the Clifford group. Nonetheless, the complexity of entanglement is generally thought of as stemming from the conjunction of a volume-law scaling for entanglement entropies and a finite magic. Indeed these properties, along with a universal entanglement spectrum statistics, have been shown to be at the root of the onset of quantum chaos [44,46–48], the hardness of disentangling algorithms [33,34,45], the universal behavior of out-of-time-order correlation functions (OTOCs) [35,49,50], and the hardness of simulatability of quantum many-body systems [38,51].

While the role of entanglement properties in quantum many-body systems has now been firmly established [7,8], it is only very recently that the connection between nonstabilizerness/magic and states produced by relevant quantum many-body physics has been the subject of investigation [51–53]. Relevant progress in this direction has been made in Ref. [43], where a novel measure of nonstabilizerness—called stabilizer Rényi entropy—has been introduced, which is experimentally measurable [54] and directly amenable to a numerical computation for quantum many-body states [53,55].

The relationship between entanglement and nonstabilizerness/magic in physically relevant quantum many-body states has first been explored in the context of quantum circuits, where efficient entangling resources can be in principle limited to the Clifford group, while magic is only produced by universal operations [33,34,56]. Indeed it has been shown that output states of random Clifford circuits possess volume law for entanglement just like Haar-random states; however, their entanglement spectrum statistics is not Wigner-Dyson distributed, but rather Poissonian. Moreover, the onset of Wigner-Dyson statistics in the output states of random universal circuits is accompanied by the appearance of universal scaling in the fluctuations of entanglement entropy, while the fluctuations of output states of random Clifford circuits display nonuniversal scaling [44,45,57]. "Simple" entanglement, associated with the absence of magic, has another relevant algorithmic consequence: an entanglement annealing algorithm, which generates a disentangling random Clifford circuit via the Metropolis algorithm, is very efficient in disentangling a state featuring simple entanglement, without any information on the circuit that generated it in the first place. On the other hand, by gradually "doping" random Clifford circuits with universal operations, such as T-gates, one can drive a transition towards a complex pattern of entanglement [44,45,57–60].

In the case of quantum many-body states which are eigenstates of a local Hamiltonian, entanglement complexity exhibits a very rich palette of possibilities. Disordered Heisenberg spin chains, corresponding to interacting 1D fermions with a random chemical potential, and featuring a many-body localization transition, have been shown [51] to exhibit two different forms of entanglement spectrum statistics. At low disorder, the model possesses high-energy eigenstates obeying the eigenstate-thermalization hypothesis (ETH) [61–65] and exhibiting a volume-law scaling for entanglement entropies. These states are also shown to feature a universal Wigner-Dyson entanglement spectrum statistics and for these states the disentangling algorithm fails. Therefore, the ETH phase corresponds to a complex-entanglement phase. Upon increasing the disorder strength, the many-body localization transition is accompanied by a violation of the Wigner-Dyson entanglement spectrum statistics and by area-law scaling of entanglement. As a result, the disentangling algorithm can achieve a significant reduction of the entanglement entropy via a random Clifford circuit, although the convergence of this algorithm for such states has not been studied. A third form of entanglement complexity is exhibited by disordered XX spin chains, corresponding to noninteracting fermions with a random chemical potential. For those systems, all states feature Anderson localization for any disorder strength, namely an area-law scaling of entanglement and concomitantly they show a Poisson entanglement spectrum statistics and are efficiently disentangled by an annealed random Clifford circuit [51].

A different picture is found instead in the ground state of paradigmatic local Hamiltonians such as the quantum Ising model: there entanglement is known to exhibit an area-law scaling, translating into a half-system entanglement entropy which is $O(1)$ in one dimension for every point of the phase diagram, except at the critical point of the ferromagnetic-paramagnetic transition [13]. However, the stabilizer entropy exhibits *always* a volume-law scaling. In such models, the critical point is special because it is the point where magic also delocalizes and cannot be resolved in terms of local quantities [53]: in the gapped phase of a chain with N qubits the magic M_L of a block of L spins would serve as a good approximation for the magic of the whole chain M_N by $M_N \simeq N/LM_L$. On the other hand, at the critical point, long-range correlations manifest themselves by an error in the approximation scaling with L^{-1}.

The ground state of the 1D quantum Ising model does not exhibit a complex entanglement pattern, as its entanglement spectrum statistics is far from the Wigner-Dyson distribution. Indeed, it features also other symptoms of simple entanglement pattern: it is efficiently disentangled by entanglement annealing [33,45] and lacks a volume-law scaling for entanglement entropy in spite of the volume-law scaling for stabilizer entropy. This is likely going to be the case for the ground states of most local Hamiltonians, given that an area-law scaling of entanglement (up to logarithmic corrections) is their characteristic feature. Moreover, even in the presence of volume-law entanglement, a volume-law scaling for the stabilizer Rényi does not imply universal entanglement spectrum statistics, but rather this scaling should be faster than a specific threshold as shown in Refs. [44,45,57].

The unifying picture emerging from these results is the following. Complex entanglement, exhibiting volume-law scaling for entanglement entropy *and* a Wigner-Dyson entanglement spectrum statistics, is a characteristic of excited Hamiltonian eigenstates satisfying ETH, as well as states prepared with random universal circuits. On the other hand, entangled states which are not complex are found as eigenstates of strongly disordered Hamiltonians, as output states of random Clifford circuits, and ground states of local Hamiltonians.

B. Probing entanglement complexity in model wavefunctions

The above emerging picture is so far only reported "piecewise" in the recent literature—namely only partial aspects of entanglement complexity have been investigated for either Hamiltonian eigenstates or output states of random circuits. In this paper we aim at a thorough investigation of entanglement complexity in a family of quantum many-body states which have the property of admitting an explicit expression for their coefficients, depending on a single parameter, and which feature a rich palette of different phases with varying entanglement complexity upon tuning the control parameter. This one-parameter family of states has the so-called Rokhsar-Kivelson (RK) form, equipped with a random sign structure (hereafter denoted as RK-sign family)—namely the wavefunction coefficients in the computational basis have amplitudes given by the Boltzmann weights of the so-called random-energy model (REM) [66] of statistical mechanics and random signs. In particular, the RK model is based on a quantum random energy model (QREM). This model can be seen as the limit $p \to \infty$ of the p-spin model (see [67]). As such, the RK model is nonlocal.

The parameter λ controlling the property of the states corresponds to the inverse temperature for the REM. These states have been first studied in Ref. [28], where they have been found to exhibit a transition from a phase possessing volume-law scaling of entanglement to a phase featuring subextensive scaling, reminiscent of many-body localization.

In this work, we show rigorously that the RK-sign states possess a transition at a critical value λ_c revealed by the fidelity metric and corresponding to the spin-glass phase transition of the REM. Nonetheless the existence of this transition is in fact independent of the sign structure of the states, while the entanglement properties are crucially dependent on such a structure. As a consequence the entanglement properties reveal a different picture, exhibiting a rich palette of different scaling regimes and complexity features. We investigate all the known complexity metrics for entanglement, namely (i) the scaling of the half-system entanglement entropy, (ii) the adherence of the entanglement spectrum statistics to the Wigner-Dyson distribution, as measured by the Kullback-Leibler divergence D_{KL}, and by the average ratio of adjacent gaps in the entanglement spectrum, (iii) the amount of nonstabilizerness measured by the stabilizer Rényi entropy M_2, (iv) the behavior of entanglement ensemble fluctuations, and (v) the hardness of factorizing by means of an entanglement annealing algorithm [33,34,45].

In agreement with Ref. [28] we find that the RK-sign states possess two scaling regimes for the half-system entanglement entropy, namely a volume-law scaling for $\lambda < \lambda_E$ and a sub-volume-law scaling for $\lambda > \lambda_E$, with $\lambda_E < \lambda_c$. The volume-law regime is characterized by the adherence of the entanglement spectrum to the Wigner-Dyson statistics, and as such it can be qualified as featuring complex entanglement; on the other hand, the sub-volume-law phase exhibits a nonuniversal entanglement spectrum statistics. Nonetheless for the whole range of parameters, encompassing the two above-cited phases, the stabilizer Rényi entropy is extensive, revealing that the entanglement of the RK states requires universal resources to be prepared. Most remarkably, within the volume-law phase a *superuniversal* regime exists for $\lambda \lesssim 0.2$, in which all complexity metrics become essentially independent of λ and take a universal behavior: the stabilizer Rényi entropy scales to its maximum possible value, the fluctuations of entanglement entropy exhibit a universal scaling to zero as in random quantum states, and the disentangling algorithm fails completely to reduce the entanglement entropy of the state. A sketch of the various entanglement regimes is given in Fig. 1.

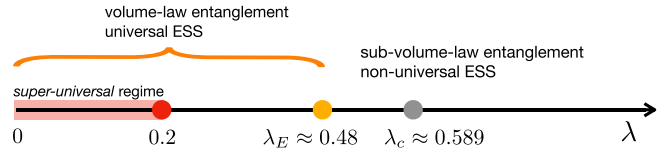

FIG. 1. Schematic diagram of the various entanglement phases we found for the RK-sign states. The entanglement transition at λ_E divides a phase with volume-law scaling of the entanglement entropy and universal (Wigner-Dyson) entanglement entropy statistics (ESS) from a phase with sub-volume-law entropies and nonuniversal ESS. A further superuniversal regime is identified within the volume-law phase.

This paper is organized as follows. In Sec. II we introduce the RK-sign family and show the existence of a singularity in the fidelity metric. In Sec. III we describe our results for the entanglement entropy scaling and its ensemble fluctuations, the entanglement spectrum statistics, the stabilizer Rényi entropy, and the efficiency of a disentangling algorithm. Conclusions and perspectives are offered in Sec. IV.

II. QUANTUM PHASE TRANSITION OF THE ROKHSAR-KIVELSON-SIGN FAMILY

A. RK-sign wavefunctions

In this section, we define the family of states dubbed RK sign and study their fidelity metric [68–70]. We consider a system of N qubits, whose Hilbert space is spanned by the computational basis $|\boldsymbol{\sigma}\rangle = |\sigma_1, \sigma_2, \ldots, \sigma_N\rangle$ of eigenstates of the σ^z Pauli operators. The RK-sign family [28,71], dependent on the parameter λ, is then defined as

$$|\psi(\lambda)\rangle = \frac{1}{\sqrt{Z(\lambda)}} \sum_{\sigma} W_{\sigma}\, e^{-\lambda E_{\sigma}} |\boldsymbol{\sigma}\rangle\,. \tag{1}$$

Here the "energies" E_{σ} obey the so-called random energy model (REM) [66], namely they are normally distributed variables with zero mean and variance $\mathrm{Var}(E_{\sigma}) = N$; the

signs $W_{\boldsymbol{\sigma}}$ are random with probabilities $p(W_{\boldsymbol{\sigma}} = \pm 1) = \frac{1}{2}$. The normalization factor contains the partition function $Z(\lambda) = \sum_{\boldsymbol{\sigma}} e^{-2\lambda E_{\boldsymbol{\sigma}}}$, namely the partition function of the REM model at inverse temperature $T^{-1} = 2\lambda$ (taking $k_B = 1$).

For $W_{\boldsymbol{\sigma}} = 1$, the above wavefunctions correspond to the so-called RK states, which are related to ground states of strongly frustrated quantum antiferromagnets [72]. On the other hand, the randomization of the sign is a necessary condition for the RK states to mimic the physics of excited eigenstates of local Hamiltonians [28,73,74], which exhibit in general a volume-law scaling of entanglement entropies. Indeed states which have random but equally signed coefficients are expected to not exhibit any scaling of the subsystem entanglement entropy [73]. Hence, in order to represent states which have entanglement complexity, a crucial ingredient of the model is the addition of random signs, potentially leading to volume-law scaling of entanglement [28,73,74].

The scaling of entanglement entropy with subsystem size in the RK-sign states is fundamentally controlled by the parameter λ, which governs the distribution of the amplitudes for the wavefunction coefficients. Entanglement entropies are found to exhibit a transition from a volume-law scaling at small λ to sub-volume-law scaling at large λ [28]. One may suspect that this transition is connected with the thermodynamic transition happening for the REM at $\lambda_c = \sqrt{2\ln 2}/2 \simeq 0.589$, at which the second derivative (the specific heat) and higher derivatives of the partition function $Z(\lambda)$ become singular. Yet, examining the scaling of Rényi entropies with different indices n for a (1/3)-(2/3) bipartition of the system, Ref. [28] concludes that the entanglement transition occurs at smaller values of λ and in a way which is dependent on the Rényi index. In Sec. III A we shall confirm this result by focusing on the von Neumann entropy (corresponding to $n = 1$) for a (1/2)-(1/2) bipartition. Nonetheless, in the remainder of this section we shall instead focus on another indicator of transitions in one-parameter families of wavefunctions, namely the fidelity metric, which can be proven rigorously to exhibit a transition at λ_c.

B. Singularity in the fidelity metric

One-parameter families of quantum states, similar to the RK-sign one, can be easily obtained as eigenstates of a quantum Hamiltonian $\mathcal{H}(\lambda)$ dependent on a parameter. Singularities in such families of states as a function of λ correspond therefore to (excited-state) quantum phase transitions of the Hamiltonian of interest. Even though we do not have a "parent" Hamiltonian for the RK-sign family, it is simple to build one mathematically (via projectors onto the states of interest) and the random nature of the RK-sign states implies that the parent Hamiltonian is a disordered one, with disorder strength controlled by λ. The transition in the RK-sign model can therefore be viewed as a disorder-induced transition in excited eigenstates of a random Hamiltonian, akin to the many-body localization transition of disordered spin models.

In order to investigate the existence of quantum phase transitions as a function of the parameter λ of the RK-sign family, one can adopt a general strategy to detect the existence of quantum phase transitions in one-parameter families of states as *singularities* in the dependence of the state properties on the parameter itself. Such a strategy is based on the behavior of the fidelity [69,75] between two nearby states parametrized by $\lambda_1 \simeq \lambda_2$, defined as $f(\lambda_1, \lambda_2) = |\langle\psi(\lambda_1)|\psi(\lambda_2)\rangle|^2$. For every λ, we can evaluate $f(\lambda, \lambda + \epsilon)$ for an infinitesimal ϵ, allowing for the expansion $f(\lambda, \lambda + \epsilon) \approx 1 - g_{\lambda\lambda}\, \epsilon^2 + o(\epsilon^3)$. The coefficient $g_{\lambda\lambda}$ is the so-called *fidelity (quantum Fisher) metric* [70,76] or *fidelity susceptibility* [77],

$$g_{\lambda\lambda} = \langle\partial_\lambda\psi|\partial_\lambda\psi\rangle - |\langle\psi|\partial_\lambda\psi\rangle|^2 \tag{2}$$

$$= -\frac{1}{2}\frac{\partial^2}{\partial\epsilon^2} f(\lambda, \lambda+\epsilon)\Big|_{\epsilon=0}, \tag{3}$$

providing a notion of distance in Hilbert space among states belonging to the one-parameter family.

Quantum phase transitions can be generically detected by a nonanalycity [78] in $g_{\lambda\lambda}$, as shown in a wide variety of recent numerical studies [69,75,79,80]. Moreover, the fidelity metric is the quantum Fisher information of the quantum state, expressing the fundamental sensitivity of the state to variations of the λ parameter and bounding the precision with which the λ parameter can be estimated by making measurement on the state. The singularity of the fidelity metric at quantum phase transitions is therefore at the root of the enhanced metrological sensitivity for parameter estimation associated with quantum criticality [81].

The fidelity metric for the RK-sign wavefunctions can be easily computed analytically and it can be directly related to thermodynamic properties of the REM—related to the amplitudes of the wavefunction coefficients. We start by observing that the λ derivative of the state vector $|\partial_\lambda\psi\rangle$ takes the form

$$|\partial_\lambda\psi\rangle = \frac{1}{\sqrt{Z}}\sum_{\boldsymbol{\sigma}}(\langle E\rangle_{\rm REM} - E_{\boldsymbol{\sigma}})W_{\boldsymbol{\sigma}} e^{-\lambda E_{\boldsymbol{\sigma}}}\,|\boldsymbol{\sigma}\rangle\,, \tag{4}$$

where $\langle E^n\rangle_{\rm REM} \equiv \frac{1}{Z}\sum_{\boldsymbol{\sigma}} E_{\boldsymbol{\sigma}}^n e^{-2\lambda E_{\boldsymbol{\sigma}}}$ is the thermodynamic average for the REM. This allows us to compute the two terms appearing in the expression of the fidelity metric, Eq. (2):

$$\langle\partial_\lambda\psi|\partial_\lambda\psi\rangle = \frac{1}{Z}\sum_{\boldsymbol{\sigma}}(\langle E\rangle_{\rm REM} - E_{\boldsymbol{\sigma}})^2 e^{-2\lambda E_{\boldsymbol{\sigma}}} \tag{5}$$

$$= \langle E\rangle^2_{\rm REM} - \langle E\rangle^2_{\rm REM}, \tag{6}$$

$$\langle\psi|\partial_\lambda\psi\rangle = \frac{1}{Z}\sum_{\boldsymbol{\sigma}}(\langle E\rangle_{\rm REM} - E_{\boldsymbol{\sigma}})e^{-2\lambda E_{\boldsymbol{\sigma}}} = 0. \tag{7}$$

Hence the fidelity metric, averaged over the ensemble of energies $\{E_{\boldsymbol{\sigma}}\}$, is equal to the energy fluctuations of the REM at inverse temperature $T^{-1} = 2\lambda$:

$$\overline{g_{\lambda\lambda}} = \langle E^2\rangle^2_{\rm REM} \equiv (\Delta^2 E)_{\rm REM}, \tag{8}$$

where $\overline{(\ldots)}$ denotes the average over the ensemble of RK-sign states at fixed λ.

The energy fluctuations of the REM are directly related to its heat capacity via the fluctuation-dissipation relation

$$C_{\rm REM} = \frac{\partial\langle E\rangle_{\rm REM}}{\partial T} = \frac{(\Delta^2 E)_{\rm REM}}{T^2}. \tag{9}$$

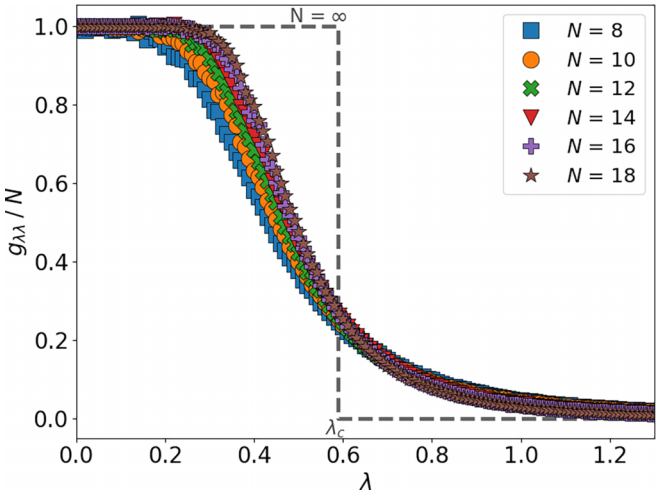

FIG. 2. Plot of the fidelity metric $g_{\lambda\lambda}$ per qubit for different system sizes. Each point is an average over $N_s = 1000$ realizations of the wavefunction. The dashed line shows the expected behavior in the thermodynamic limit.

In turn the heat capacity of the REM is analytically known [66,82] to exhibit a jump singularity at the transition of the model:

$$C = \begin{cases} 0, & T < T_c, \\ \frac{N}{T^2}, & T > T_c, \end{cases} \tag{10}$$

with $T_c = 1/\sqrt{2\ln 2}$ [83]. This immediately implies that the fidelity metric of the RK-sign family $\overline{g_{\lambda\lambda}} = T^2 C_{\mathrm{REM}}$ inherits the singularity of the specific heat of the REM model at $\lambda_c = 1/(2T_c) = \sqrt{2\ln 2}/2$ in the form of a simple step-function singularity:

$$\overline{g_{\lambda\lambda}} = \begin{cases} 0, & \lambda > \lambda_c, \\ N, & \lambda < \lambda_c. \end{cases} \tag{11}$$

The above analytical calculation is strictly valid only in the thermodynamic limit $N \to \infty$. It is instructive to examine finite-size effects by computing $g_{\lambda\lambda}$ numerically on finite-N wavefunctions via the finite-element derivative formula:

$$g_{\lambda\lambda} = -\frac{1}{2}\frac{f(\lambda, \lambda + 2\epsilon) - 2f(\lambda, \lambda + \epsilon) + 1}{\epsilon^2}. \tag{12}$$

For every realization of $W_{\boldsymbol{\sigma}}, E_{\boldsymbol{\sigma}}$, we compute $g_{\lambda\lambda}$ and average it over $N_s = 1000$ realizations. In Fig. 2 we show the behavior of $\overline{g_{\lambda\lambda}}$ for different system sizes $N = 8, \ldots, 18$. The curves of $\overline{g_{\lambda\lambda}}/N$ for different values of N are found to cross in the vicinity of the critical value λ_c, consistent with the existence of a jump in the thermodynamic limit. To reconstruct the position of the critical point λ_c from finite-size scaling, we analyze the derivatives of $g_{\lambda\lambda}$ for our finite systems. For each N, we consider the polynomial that fits the points of $g_{\lambda\lambda}$ as a function of λ. Then, we take the first derivative of these polynomials and identify the minimum points $\lambda_M(N)$ [Fig. 3(a)]. We fit the minima $\lambda_M(N)$ to an exponential curve of the form $A\exp(-B/N) + C$, such that $\lambda_M(N \to \infty) = A + C$. This scaling law is phenomenological, but it is strongly suggested by our data [as shown in Fig. 3(b)] and the extrapolated value of λ_M, $\lambda_M(\infty) = 0.588 \pm 0.013$ is in quantitative agreement

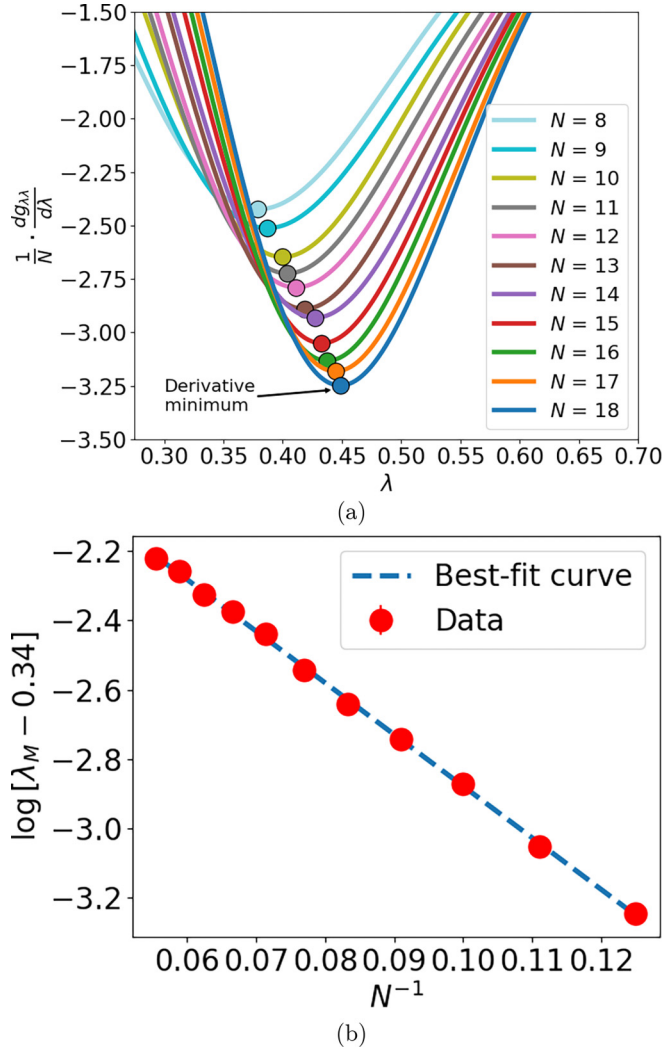

FIG. 3. (a) First derivatives of the polynomials used to fit $g_{\lambda\lambda}/N$, for different system sizes N: the dots mark the minima $\lambda_M(N)$ of each curve. (b) Localization of the critical point λ_c through finite-size scaling: the minima $\lambda_M(N)$ are fitted to an exponential curve of the form $\lambda_M(N) = A\exp[\frac{-B}{N}] + C$. A χ^2-minimization approach [84] gives $A = 0.249 \pm 0.005$, $B = 14.9 \pm 1.4$, $C = 0.339 \pm 0.007$, and λ_c is extrapolated to infinite size as $N^{-1} \to 0$. The results are plotted here on a semilogarithmic scale, where a linear trend ($R^2 \approx 0.9994$) emerges.

with the REM transition point $\lambda_c = \sqrt{2\ln 2}/2 \simeq 0.589$. This scaling analysis highlights the fact that finite-size effects are very strong for the system sizes we considered.

III. ENTANGLEMENT COMPLEXITY TRANSITION

In this section, we examine the quantum phase transition of the RK-sign family from the point of view of entanglement complexity, computing the behavior of different complexity metrics as a function of the parameter λ. More precisely, we will compute the entanglement entropy for a subsystem with $N/2$ qubits, the entanglement spectrum statistics, the stabilizer Rényi entropy, the ensemble fluctuations of the entanglement entropy, and the disentangling power of a Metropolis algorithm.

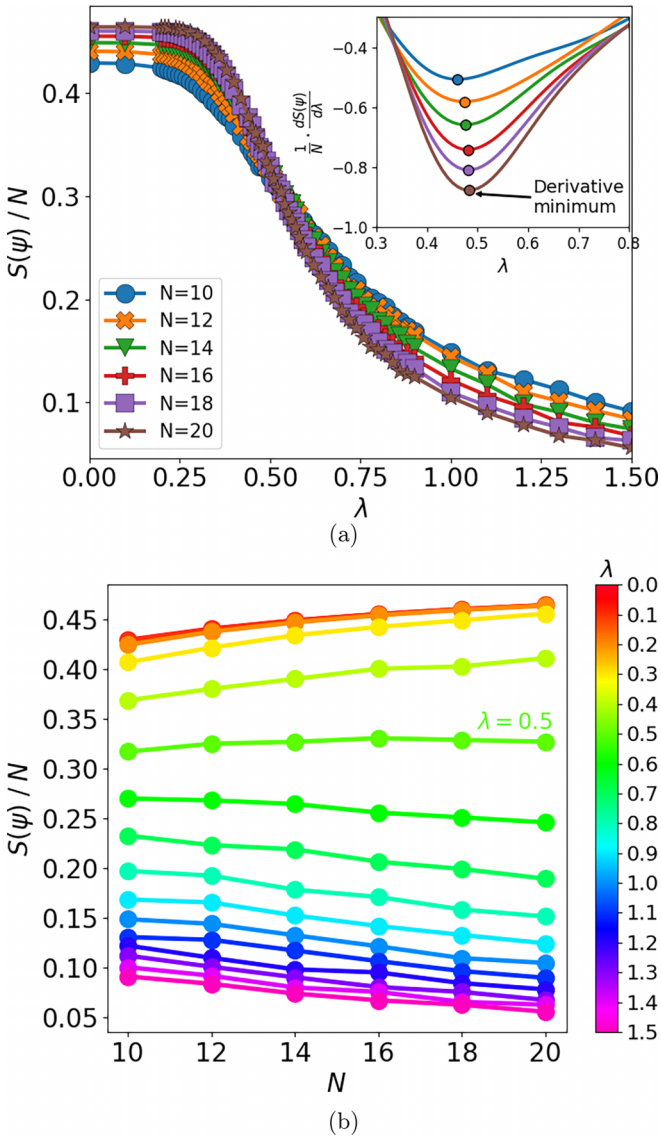

FIG. 4. (a) von Neumann entanglement entropy $S(\psi)$ per qubit as a function of λ, for different system sizes N. In the inset, first derivative of the best-fit curves for $S(\lambda)$; the dots mark the minimum of each curve. (b) $S(\psi)/N$, as a function of N, for different λ in the interval [0,1.5].

A. Scaling of entanglement entropy

For every state $|\psi(\lambda)\rangle$ we consider an equal bipartition into two groups of $N/2$ qubits and calculate the von Neumann entropy of the reduced density matrix of the half system $S_{N/2}(\psi) = -\mathrm{Tr}(\rho_{N/2}\log_2\rho_{N/2})$, where $\rho_{N/2} = \mathrm{Tr}_{N/2}|\psi\rangle\langle\psi|$. The half-system entropies are then averaged over a sample of size N_s of RK-sign states to give the results shown in Fig. 4. There we observe that, upon increasing λ, a clear transition takes place between a phase with volume-law scaling of entanglement at low λ and a phase with subextensive scaling. In fact, the low-λ phase appears to exhibit superextensive scaling, but this can only be a finite-size effect, as extensive scaling is the fastest one allowed for entanglement entropy. Moreover, the volume-law phase remarkably contains a regime for $\lambda \lesssim 0.2$ where the entanglement entropy is constant, a feature that will be common to other figures of merit examined in this work.

The location of the transition between the two scaling regimes (volume law vs subextensive scaling) can be in principle deduced from the position of the minimum derivative of the $S_{N/2}/N$ curves: indeed, regardless of the specific scaling dimension of the entanglement entropy at the transition, one can generally expect that the critical point be marked by the strongest decrease of $S_{N/2}$ upon varying the control parameter. The inset of Fig. 4(a) shows that the minimum derivatives exhibit little scaling in position and indicate an entanglement transition at $\lambda_E \approx 0.48 < \lambda_c$. While this estimate might still be affected by significant finite-size corrections, our conclusion (entanglement transition preceding the REM transition) is in agreement with the findings of Ref. [28]. In fact it is easy to understand why the two transitions should be independent, based on rather general arguments. As we have seen in Sec. II B, the fidelity metric is uniquely sensitive to the *amplitudes* of the wavefunction coefficients and their λ dependence—namely on the localized vs delocalized nature of the wavefunctions when expressed on the computational basis. On the other hand, as shown in Ref. [73], the sign structure of the coefficients is crucially important in determining the scaling of the entanglement entropy: if one considered, e.g., positive-definite coefficients, all RK states would exhibit a sub-volume-law scaling of entanglement entropy. This means that different sign distributions for the coefficients (less random than the one adopted here) can move the entanglement transition of the RK-sign family or make it disappear altogether, while by construction the fidelity-metric transition remains insensitive to these features. Hence the entanglement transition and the REM transition are necessarily decoupled. This observation may look surprising, but in fact changes in the behavior of the entanglement pattern are not always accompanied by a singularity in the fidelity metric related to a QPT [17,85]. As an example, Ref. [86] shows that the ground-state factorization occurring in the XYZ model in a field, albeit providing a special behavior in the entanglement properties, does not show any singularity in the fidelity metric related to the ground-state wavefunction.

B. Entanglement spectrum statistics

In this section we examine the entanglement spectrum statistics, which has been pointed out as a fundamental indicator of entanglement complexity in Refs. [33,34,56]. Considering the eigenvalues of the half-system reduced density matrix $\{a_i\}$ $(i = 1, \ldots, 2^{\frac{N}{2}} - 1)$ in increasing order $a_i < a_{i+1}$, we define the gaps between adjacent eigenvalues $\delta_j = a_{j+1} - a_j$, as well as the two different ratios of adjacent gaps:

$$r_k = \frac{\delta_{k+1}}{\delta_k}, \tag{13}$$

$$\tilde{r}_k = \frac{\min[\delta_{k+1}, \delta_k]}{\max[\delta_{k+1}, \delta_k]}. \tag{14}$$

We then focus on the gap-ratio distribution $P(r)$ and on the average gap ratio $\langle\tilde{r}\rangle$, built from the gaps of all the density matrices associated with a sample of RK-sign states (of size $N_s = 1000$) upon varying the λ parameter.

It has been shown [34,56] that complex entanglement is associated with level repulsion in the entanglement spectrum and, specifically, with the emergence of Wigner-Dyson (WD) statistics, namely the distribution of gap ratios [87]

$$P_{\rm WD}(r) = \frac{1}{Z}\frac{(r+r^2)^\gamma}{(1+r+r^2)^{1+\frac{3}{2}\gamma}}. \tag{15}$$

This distribution of gap ratios is associated with random matrices belonging to the Gaussian orthogonal ensemble (GOE) (for which $\gamma = 1$ and $Z = \frac{8}{27}$), as well as the Gaussian unitary ensemble (GUE) (for which $\gamma = 2$ and $Z = \frac{4\pi}{81\sqrt{3}}$) [88]. In our case of interest, the reduced density matrix is real valued (as are the wavefunction coefficients) so that the relevant ensemble is expected to be the GOE. On the other hand, "simple" entanglement is associated with departure from the Wigner-Dyson statistics and the emergence of alternative statistics not showing level repulsion—the simplest case being Poisson's statistics, associated with random eigenvalues, resulting in a gap-ratio distribution $P_{\rm Poisson}(r) = (1+r)^{-2}$ [89].

In Fig. 5 the gap-ratio distribution $P(r)$ (blue stars) is shown for two different values of λ on the two sides of the entanglement transition. For $\lambda = 0$ ($< \lambda_E$) we see that the gap distribution agrees well with the GOE Wigner-Dyson form, as expected from a complex-entanglement phase. On the other hand, for $\lambda = 1.5$ ($> \lambda_E$), the distribution strays away from the Wigner-Dyson form, although it is not complying either with Poisson statistics.

To quantify the discordance between the gap-ratio distribution $P(r)$ of the RK-sign states and that resulting from Wigner-Dyson statistics, $P_{\rm WD}(r)$, we evaluate the Kullback-Leibler divergence between the two distributions

$$D_{\rm KL}[P(r)||P_{\rm WD}(r)] = \sum_k P(r_k)\ln[P(r_k)/P_{\rm WD}(r_k)]. \tag{16}$$

We show $D_{\rm KL}$ as a function of λ in Fig. 6(a) for different system sizes, along with an extrapolation to the thermodynamic limit. As one can see, for $\lambda \lesssim \lambda_E$, $D_{\rm KL}$ extrapolates to zero in the thermodynamic limit. Upon crossing the transition, $D_{\rm KL}$ becomes finite: this suggests that the entanglement transition of the RK-sign states is marked by a sharp shift in the entanglement spectrum statistics, namely it is accompanied by a sharp transition in entanglement complexity as well.

Another way to quantify the discordance of the entanglement spectrum statistics with the Wigner-Dyson statistics is to evaluate the average $\langle\tilde{r}\rangle$ defined in Eq. (14). This average can be used as a direct indicator of the specific statistics followed by the entanglement spectrum, as it takes the value $\langle\tilde{r}\rangle \approx 0.53$ for the GOE, whereas, e.g., for Poisson statistics one has the value $\langle\tilde{r}\rangle \approx 0.39$ [90]. $\langle\tilde{r}\rangle$ is plotted as a function of λ in Fig. 6(b), where one can see that for a certain λ_r the phase with $\lambda < \lambda_r$ is essentially consistent with the GOE statistics, while for $\lambda > \lambda_r$ there is a gradual departure from GOE behavior. The exact value of λ_r at which this departure happens cannot be estimated precisely, due to the residual noise in $\langle\tilde{r}\rangle$ close to the transition. Our calculations show that $\langle\tilde{r}\rangle(\lambda = 0.44) = 0.528 \pm 0.003$ and $\langle\tilde{r}\rangle(\lambda = 0.5) = 0.524 \pm 0.002$, allowing us to locate the transition point in this interval of λ values. This result is compatible with the value of the entanglement transition $\lambda_E \approx 0.48$ and leads us to consider the two points as equivalent: $\lambda_r \simeq \lambda_E$. These metrics suggest therefore that the whole volume-law phase of the RK-sign states exhibits universal Wigner-Dyson statistics of the entanglement spectrum.

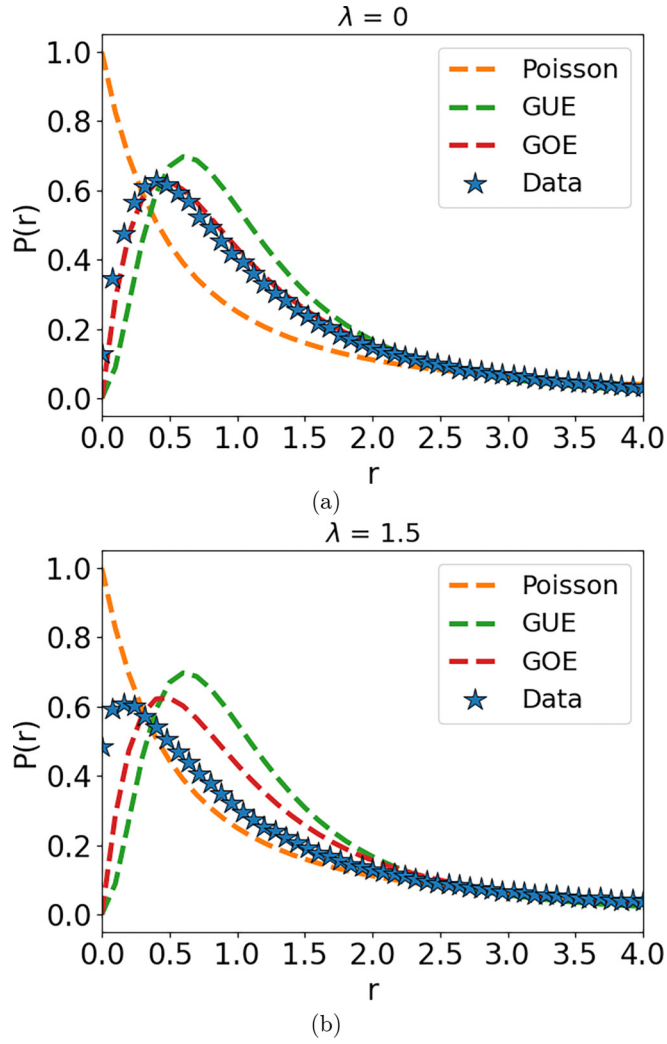

FIG. 5. Comparison between the distribution $P(r)$ for the gaps of the entanglement spectrum of $N = 18$ qubits and known statistical distributions (GOE, GUE, and Poisson—see text), for two different values of λ: (a) $\lambda = 0$; (b) $\lambda = 1.5$.

C. Ensemble fluctuations of the entanglement entropy

References [44,45,57] have shown that another signature of entanglement complexity in an ensemble of wavefunctions is offered by ensemble entanglement-entropy fluctuations. Following the analysis of the above-cited references, we define the variance of sample-to-sample fluctuations of the half-system entanglement entropy

$$\mathrm{Var}(S_{N/2}) \equiv \overline{S^2_{N/2}(\psi)} - \overline{S_{N/2}(\psi)}^2, \tag{17}$$

where again the symbol $\overline{(\ldots)}$ represents the average over a number N_s of samples (here, $N_s = 1000$).

Figure 7 shows the variance of the half-system entanglement entropy as a function of λ; a peak appears for intermediate λ getting sharper with increasing system size and moving to lower values of λ. While a scaling analysis of the

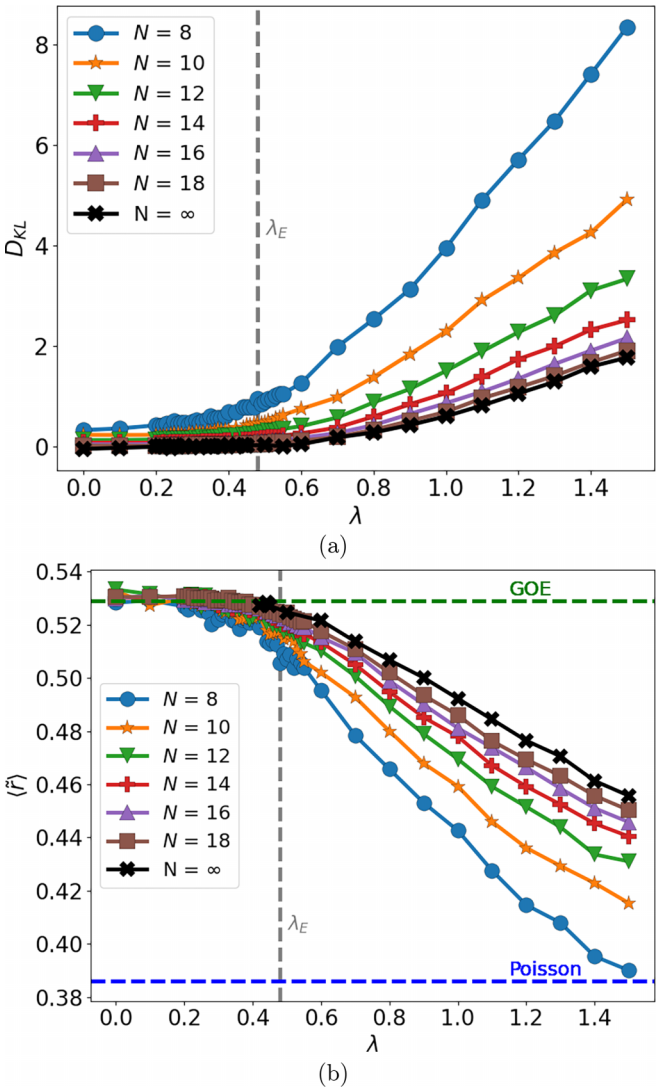

FIG. 6. Entanglement spectrum statistics of the RK-sign wavefunctions as a function of λ: (a) Kullback-Leibler divergence D_{KL} between the RK-sign distribution of gap ratios and the one stemming from Wigner-Dyson statistics. The dashed vertical line marks the critical value λ_E; (b) $\langle \tilde{r} \rangle$ as a function of λ, compared with the corresponding values for the GOE statistics (≈0.53) and the Poisson statistics (≈0.39). All results are obtained from a pool of 1000 RK-sign wavefunctions.

peak position is rendered complicated by the noisy nature of the variance extracted from limited statistics, it appears rather plausible that the peak position drifts towards the entanglement transition at λ_E. Moreover, the peak clearly separates rather sharply two scaling regimes: one of very slow scaling of the variance upon increasing the system size at small λ and another one of much faster scaling at large λ.

The scaling ansatz capturing the size dependence of the variance across the entire parameter range reads as

$$\mathrm{Var}(S_{N/2}/N) \propto d^{-\theta}, \tag{18}$$

where $d \equiv 2^N$ is the Hilbert-space dimension. The exponent θ can then be obtained from a linear fit of $\log_2[\mathrm{Var}(S_{N/2}/N)]$ vs N—examples of such fits are shown in Fig. 8(a) for two values

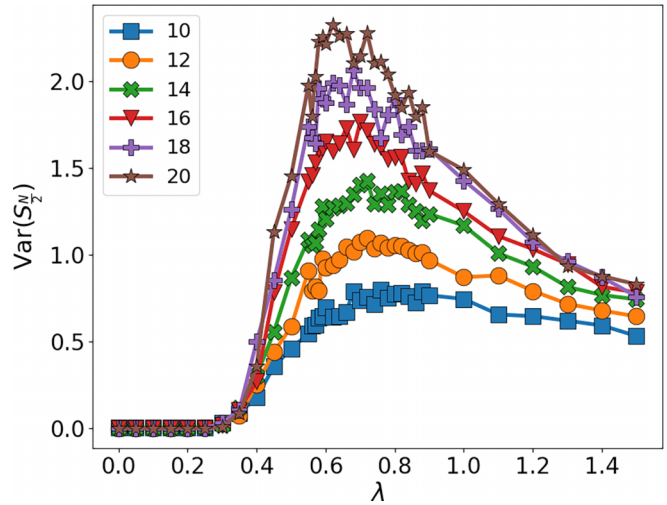

FIG. 7. Entanglement-entropy fluctuations of the half-bipartition of the system, as functions of λ, for different system sizes. The averages computed in the derivation of $\mathrm{Var}(S_{N/2})$ are obtained from a pool of 1000 samples.

of λ, providing widely different values of θ between the $\lambda < \lambda_E$ regime and the $\lambda > \lambda_E$ regime. Figure 8(b) puts together the values of the θ exponent obtained for different values of λ. In particular, two asymptotic regimes emerge: one for $\lambda \lesssim 0.2$ with $\theta \approx 1.2$ and one for $\lambda \gtrsim 1.5$ with $\theta \approx 0.14$. The first regime is in fact rather remarkable, as it exhibits a *universal* scaling of entanglement entropy fluctuations consistent with that of the output states of random quantum circuits, for which $\theta \sim 1.25$ [45]. These two regimes are separated by a sharp drop in θ which marks the transition for $\lambda \approx \lambda_E$, accompanied by the slowest scaling. This behavior is clearly reflected in the appearance of the peak in Fig. 7.

D. Stabilizer Rényi entropy

As we have seen in the previous sections, the entanglement transition of the RK-sign states—from volume-law scaling to subextensive scaling—is accompanied also by a transition in entanglement complexity as revealed by the entanglement spectrum statistics. A similar phenomenology has been observed for the high-energy excited states of the disordered XXZ model [51]. Nonetheless, it is important to remark that volume-law scaling for entanglement is not necessarily connected to a complex pattern of entanglement, as it has been shown in a series of works [33,34,44,51,56,91]. For instance, the output of a random quantum circuit made of Clifford gates features volume-law scaling for entanglement, but it exhibits Poisson entanglement spectrum statistics and nonuniversal fluctuations for the entanglement entropy [44,45]. The above example refers to states that have been produced with Clifford-group gates; therefore, a direct way to tell apart such states with respect to the RK-sign ones is to probe the nonstabilizerness/magic of the latter. In order to do so, we consider the entropy associated with the probability distribution over the Pauli decomposition of a state—the so-called stabilizer Rényi entropy [43], which quantifies explicitly nonstabilizerness.

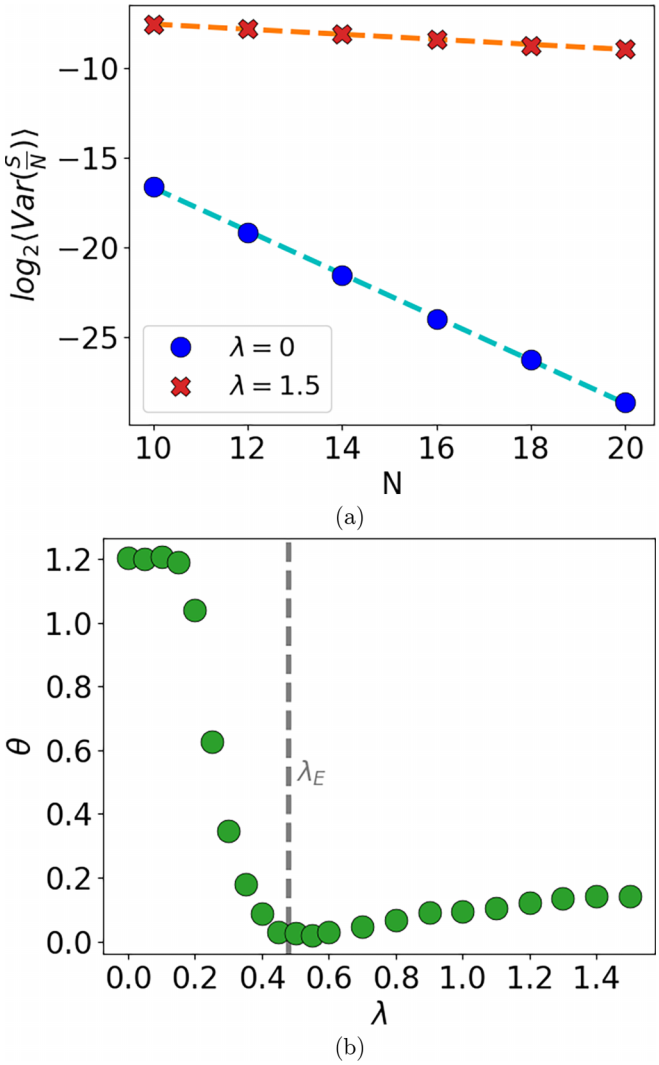

FIG. 8. (a) Scaling of the entanglement entropy ensemble fluctuations with system size, fitted to the scaling ansatz $\log_2[\mathrm{Var}(S_{N/2})/N] = -\theta N + \mathrm{const}$, for two values of λ. The dashed lines represent the best-fit lines for each choice of λ: if $\lambda = 0$, one finds $\theta = 1.205 \pm 0.009$, whereas, if $\lambda = 1.5$, one finds $\theta = 0.140 \pm 0.006$. (b) Exponent θ for the scaling of entanglement-entropy fluctuations as a function of λ.

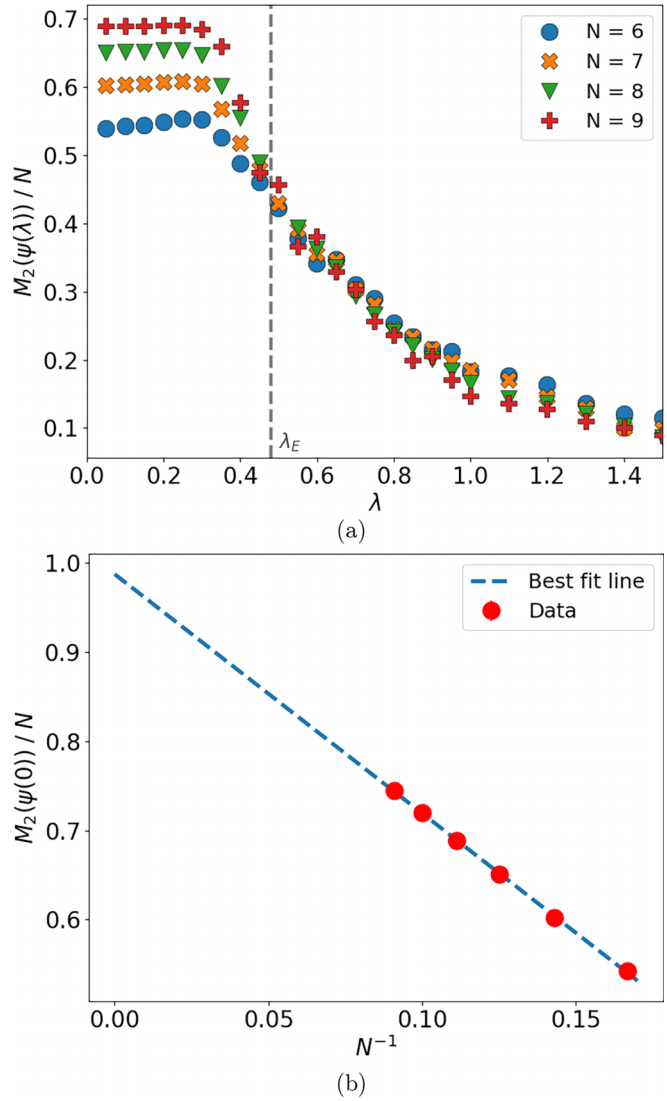

FIG. 9. (a) Stabilizer Renyi entropy M_2 per qubit as a function of λ, for different system size; each point is computed averaging over $N_s = 400$ samples. (b) Scaling of stabilizer Renyi entropy per qubit at $\lambda = 0$. The system size N goes from 6 to 11. The number of realizations N_s is 25 for $N = 11$ and 400 otherwise. $R^2 = 0.9996$ [92] indicates a good linear fit. The intercept of the best-fit line represents the value of $M_2(0)$ in the thermodynamic limit: $M_2(0) \simeq 0.99N$.

The stabilizer 2-Rényi entropy is defined as follows: consider the set $\mathcal{P}$ of all operators obtained from the tensor product of N single-qubit Pauli gates—that is, $\mathcal{P} = \{\mathbb{I}, X, Y, Z\}^{\otimes N}$. If P_n $(n = 1, \ldots, 4^N)$ are the elements of $\mathcal{P}$, then the stabilizer 2-Rényi entropy M_2 of any pure state $|\psi\rangle$ is given by

$$M_2(|\psi\rangle) = -\log_2 \sum_{n=1}^{4^N} \left(\frac{\langle\psi| P_n |\psi\rangle^2}{2^N} \right)^2 - N. \qquad (19)$$

Note that the computation of this quantity requires one to evaluate 4^N expectation values of $2^N \times 2^N$ operators and that, for each value of λ, the random nature of the RK-sign states requires that we also average the result over several (N_s) samples. This means that $M_2(\lambda)$ requires significantly longer computation times with respect to other quantities that have been considered earlier in this work. It is therefore computationally expensive to reach the same system sizes as those considered in the previous sections and to provide a proper finite-size scaling analysis. Nonetheless, already the accessible sizes we could consider $(N = 6, 7, 8, 9)$ provide a suggestive picture of the behavior of nonstabilizerness in the RK-sign states, as shown in Fig. 9(a). There the curves of M_2/N appear to exhibit a superextensive scaling for sufficiently low λ—which, similar to the entanglement entropy, must necessarily turn into extensive scaling at larger N, as one can prove that $M_2 \leqslant N$ for N qubits [43]. In fact, as shown in Fig. 9(b), for $\lambda = 0$ we can show that M_2/N extrapolates to a value close to 0.99, nearly saturating its upper bound. We argue that this scaling behavior should persist over the entire regime $\lambda \lesssim 0.2$, given that the stabilizer Rényi entropy

is essentially independent of λ over this λ range for all the system sizes we considered.

Increasing the value of λ, the M_2/N curves are found to drop to smaller values, with a maximum λ derivative (in absolute value) corresponding roughly to λ_E. Nonetheless, even upon entering the sub-volume-law phase, the scaling of the stabilizer Rényi entropy appears to maintain a volume law. The coexistence between an extensive stabilizer Rényi entropy and subextensive entanglement entropy is not surprising and it has been observed in the ground state of the quantum Ising chain [53].

E. Disentangling hardness

A final, more heuristic probe of the complexity of entanglement featured by the RK-sign states is offered by the efficiency of disentanglement using an entanglement annealing algorithm. Within this algorithm, the RK-sign states are evolved with a Clifford circuit stochastically built as follows. The random extraction of a single qubit gate (Hadamard gate, S gate) or a two-qubit (CNOT) gate is put to a Metropolis-algorithm test: namely, if the gate leads to a decrease in entanglement entropy across the average over all the half-system bipartitions, then the gate is retained. If instead the entanglement entropy increases by a ΔS, then the gate is retained with a Metropolis-Hastings algorithm scheme, namely with a probability of acceptance given by $p = \exp(-\beta \Delta S)$. Here β is a fictitious inverse temperature, which is a parameter of the algorithm and which can be a function of the annealing step (defining the so-called annealing schedule). The detailed scheme of the algorithm can be found in Refs. [34,45].

Several recent works have shown a link between entanglement complexity of a state and hardness to disentangle it with the above-cited algorithm. In Refs. [33,34,45,56,57] on random quantum circuits, the presence of magic in the quantum states—obtained for example by inserting T gates in the random circuit—is found to lead to output states of the circuit exhibiting Wigner-Dyson entanglement spectrum statistics. And, in turn, the same states are found to be hard to disentangle using the entanglement annealing algorithm—namely the maximum amount of reduction of the von Neumann entropy in a given bipartition that can be obtained by the annealing algorithm is small compared to the initial entropy. A similar phenomenon accompanies the ETH-MBL transition in disordered systems, as shown in Ref. [51].

Based on the above-cited works, we apply the disentangling-hardness diagnostics to the RK-sign states, expecting it to evolve significantly when moving across the entanglement transition. Introducing the initial half-system entanglement entropy (S_i) and the final one (S_f) after the disentangling procedure, we define the efficiency of the algorithm via the relative disentangling performance:

$$\eta(\lambda) = 1 - \overline{S_f/S_i}, \tag{20}$$

where the symbol $\overline{(\ldots)}$ indicates again the average over a number N_s of extractions of the initial state and subsequent realization of the annealing algorithm. In the following we take $N_s = 200$, at which we observe a convergence of the averaged disentangling performance with the size of the sample.

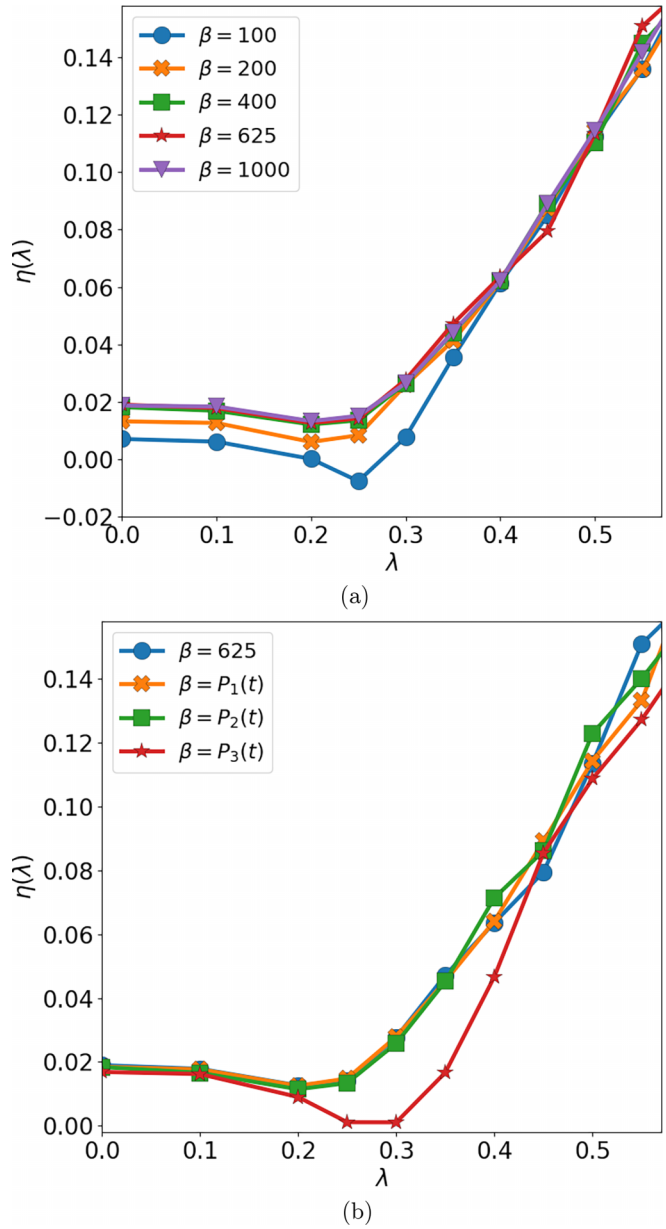

FIG. 10. Efficiency η of the disentangling algorithm applied to RK-sign states with $N = 12$ qubits. (a) Constant-β schedules, with different β values. (b) Variable-β schedules: blue (const): $\beta(t) = \beta_0$; orange: $\beta(t) = P_1(t) = \beta_0(t+1)^{0.1}$; green: $\beta(t) = P_2(t) = \beta_0 + 7.1\times10^{-6}t^2$; red: $\beta(t) = P_3(t) = \beta_0 + 1.2\times10^{-5}t^2$. In both panels, the algorithm has a total duration of $t_{\mathrm{MAX}} = 7200$ steps and the averages are performed over a sample of size $N_s = 100$.

The performance of the annealing algorithm depends in principle on (1) the annealing schedule, namely the variation of the effective inverse temperature β with the number of annealing steps, and (2) the total number of annealing steps t_{MAX} and its scaling with system size. Our results indicate nonetheless that, in the $\lambda \lesssim 0.2$ regime, the efficiency of the algorithm remains very low, regardless of its parameters.

Figure 10 shows $\eta(\lambda)$ for different annealing schedules, namely for various values of β being held constant [Fig. 10(a)] and for different power-law annealing schedules in the form

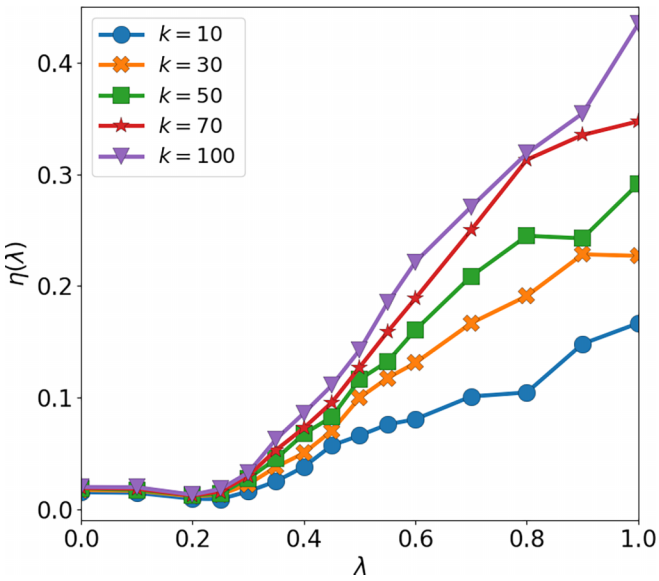

FIG. 11. Dependence of the disentangling efficiency on the annealing schedule duration $t_{\mathrm{MAX}} = kN^2$. Here $N = 12$ and $N_s = 200$.

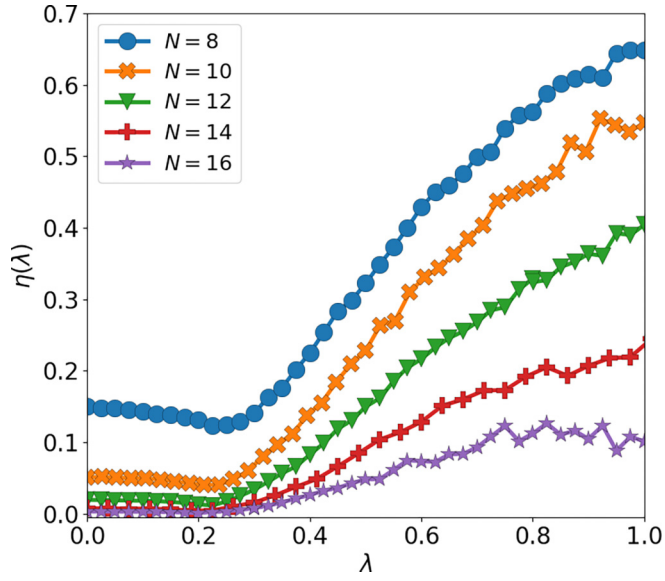

FIG. 12. Dependence of the disentangling efficiency on system size for the constant-β schedule. Here $N_s = 200$ and $t_{\mathrm{MAX}} = 100N^2$.

$\beta(t) = \beta_0 + \beta_1 t^\alpha$ in Fig. 10(b). We observe that, regardless of the specific annealing schedule—the length being fixed—its performance remains very low in the small λ regime on which the figures focus. In particular the performance is minimal and nearly independent of λ for $\lambda \lesssim 0.2$, which corresponds to a plateau regime for the entanglement entropy [Fig. 4(a)], the scaling of entanglement fluctuations (Fig. 8), and the stabilizer Rényi entropy (Fig. 9). Given the small sensitivity on the annealing schedule, in the following we shall concentrate on the simplest, constant-β scheme; in particular in Fig. 10(a) we observe that the disentangling efficiency stops increasing with β for $\beta \gtrsim 400$; hence in the following we will consider $\beta = 400$, as this value falls in the regime that shows the saturation in efficiency.

As for the dependence on the overall length of the annealing schedule, following [33,34,45] we take $t_{\mathrm{MAX}}(N)$ to scale as $t_{\mathrm{MAX}} = kN^2$, where k is constant. In Fig. 11 we plot $\eta(\lambda)$ for different values of k, observing again that for $\lambda \lesssim 0.2$ there is nearly no dependence of the disentangling efficiency on the length of the annealing protocol, while for larger values of λ the efficiency goes up with k—marking a regime of partial disentanglement—but the k dependence becomes weak for $k \approx 100$. A final remark concerns the size dependence of the disentangling efficiency: Fig. 12 shows that, when the annealing duration scales in the same way with N^2, the disentangling efficiency strongly decreases with increasing system size; in particular, for $\lambda \lesssim 0.2$, the efficiency is found to rapidly scale to zero upon increasing N.

In conclusion, we observe that the disentangling efficiency is a good indicator of the higher complexity of entanglement of the RK-sign states for small λ compared to those at large λ. Neither the fidelity-metric transition at λ_c nor the entanglement transition at λ_E seem to affect the λ dependence of the annealing efficiency. Yet the overall behavior reveals again a special regime for $\lambda \lesssim 0.2$ in which the annealing efficiency is very weakly dependent on any parameter of the annealing schedule (including its duration) and it rapidly falls to zero with system size. On the other hand, longer entanglement annealing schedules lead to a larger disentangling efficiency in the complementary $\lambda \gtrsim 0.2$ regime.

F. Superuniversal regime

As seen in the previous sections, for $\lambda \lesssim 0.2$ we observe a superuniversal regime, namely a regime in which the ensemble of states belonging to the RK-sign family exhibits an average entanglement, entanglement fluctuations, and magic which scale in a way very similar to that of the ensemble of random states in Hilbert space. Such states can be thought of as generated from a same reference state (say all N spins up), which is acted upon by a unitary which is random in the sense of the Haar measure. Similarly one can view the RK-sign states as generated via random unitaries distributed according to a different measure than the Haar measure (hereafter called RK-sign measure). In this section we attempt a more detailed comparison of the RK-sign measure with the Haar measure, aiming at better characterizing the superuniversal regime and contrasting it with respect to the regimes at larger λ.

First of all, we can understand the similarity between the statistical properties of the RK-sign states at small λ and the ones of random states by noticing that, in the limit $\lambda \to 0$, $|\psi(\lambda)\rangle$ is a superposition of all possible basis configurations with equal amplitudes and random signs. The amplitudes of the wave-function coefficients are fixed and the phase of the coefficients is extracted out of a bimodal distribution (with values 0 or π) instead of a fully flat one (on $[0, 2\pi]$). Yet this appears to be sufficient in order to reproduce the above-cited scaling of entanglement and magic properties of fully random states. In particular, this observation strongly suggests that the randomization of amplitudes is irrelevant for entanglement complexity and that its defining aspect is phase randomization.

Moving beyond these qualitative observations, we compare the Haar-measure ensemble with the RK-sign ensemble by

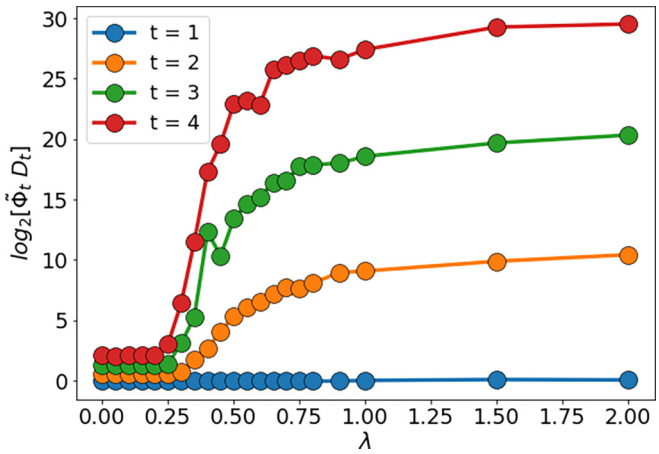

FIG. 13. Logarithm of $\tilde{\Phi}_t(\{\psi_i(\lambda)\})D_t$ as a function of λ, for different values of the moment index ($t = 1, \ldots, 4$). Each data point corresponds to an ensemble of $K = 1000$ realizations of RK-sign states of $N = 12$ qubits.

evaluating whether the latter makes up for an approximate t design [93], namely, whether the RK-sign measure is capable of reproducing the statistics of the Haar measure of up to the tth moment. As it has been shown in Ref. [44], an important threshold is that of $t = 4$, which sharply discriminates the Clifford group from the Haar measure and it is at the onset of quantum chaos. The ensemble $\{|\psi_i(\lambda)\rangle\}_{i=1}^K$—with K the number of samples—is a (projective) t design if and only if its tth frame potential, defined as [93]

$$\Phi_t\left(\{\psi_i(\lambda)\}_{i=1}^K\right) = \frac{1}{K^2}\sum_{j,k}|\langle\psi_j|\psi_k\rangle|^{2t} \tag{21}$$

attains the value

$$\Phi_t\left(\{\psi_i(\lambda)\}_{i=1}^K\right) = D_t^{-1} \equiv \binom{d+t-1}{t}^{-1}, \tag{22}$$

where $d = 2^N$ is the dimension of the Hilbert space. In general, one has $\Phi_t(\{\psi_i(\lambda)\}_{i=1}^K) \geqslant {D_t}^{-1}$. An ensemble with the property $D_t\Phi_t \simeq 1$ realizes an approximate t design. On the contrary, high values of the product $D_t\Phi_t$ denote low randomness of the ensemble of wave functions.

The off-diagonal contributions to Φ_t can be written as $\tilde{\Phi}_t(\{\psi_i(\lambda)\}_{i=1}^K) = \Phi_t(\{\psi_i(\lambda)\}_{i=1}^K) - K^{-1}$. Numerical evaluation shows that the number $\tilde{\Phi}$ converges rapidly with K, which means that it also well represents the limit $K \to \infty$ for the frame potential Φ_t.

In Fig. 13 we plot the logarithm of $\tilde{\Phi}_t(\{\psi_i(\lambda)\}_{i=1}^K)D_t$ for a sample $\{\psi_i(\lambda)\}_{i=1}^K$ of $K = 1000$ realizations of RK-sign states of $N = 12$ qubits, as a function of λ, and for different values of the moment t. As we can see, the superuniversal region shows a constant behavior of the t-frame potential, which has the same order of magnitude of the value for a 4 design. In this sense this is an approximate 4 design. In comparison, as one crosses over away from the superuniversal region, the value of $D_t\Phi_t$ rapidly increases to very high values, as one can see from a logarithmic scale; see Fig. 13. This signals a marked departure from a projective t design—the more pronounced the higher the moment t.

We observe therefore that the the superuniversal regime features high (albeit imperfect) randomness of the ensemble of wavefunctions, together with a nearly perfect independence of such randomness with respect to the parameter λ.

IV. DISCUSSION

In summary, our analysis of the entanglement features of the RK-sign wavefunctions shows that this family of states possesses an entanglement transition decoupled from that of the fidelity metric and separating a volume-law phase, characterized by universal Wigner-Dyson statistics for the entanglement spectrum, from a sub-volume-law phase with nonuniversal entanglement spectrum statistics. Within the volume-law phase a superuniversal regime appears characterized by universal entanglement entropy fluctuations, stabilizer Rényi entropy scaling towards its theoretical maximum, and close-to-null efficiency of a disentangling algorithm. These results show that the RK-sign states showcase a very rich palette of different levels of entanglement complexity, essentially encompassing all the regimes observed previously piecewise in various model systems—from the output states of random quantum circuits to ground and excited states of many-body Hamiltonians.

The phenomenology unveiled here in a one-parameter family of model quantum states may be expected to appear in the entanglement features of excited Hamiltonian eigenstates—a strong candidate being the excited states of disordered Hamiltonians featuring a many-body localization transition. A systematic study of entanglement complexity metrics for such states (and in particular of the stabilizer Rényi entropy), going beyond the analysis offered by Ref. [51], appears therefore as a rather appealing perspective. Nonetheless it is important to underline the significant computational overhead required to extract the stabilizer Rényi entropy of quantum states; on the technical side, more efficient approaches may be envisioned to calculate it, based, e.g., on a stochastic sampling of the Pauli decompositions of a state.

ACKNOWLEDGMENTS

S.P. and A.H. acknowledge support from NSF Award No. 2014000, as well as the hospitality of the "Laboratoire de Physique" of the ENS of Lyon, where part of this work was performed. The work of S.P. was supported in part by College of Science and Mathematics Dean's Doctoral Research Fellowship through fellowship support from Oracle, Project ID R20000000025727. S.P. would also like to thank L. Leone and S. F. E. Oliviero for providing helpful discussions in the production of this work. T.R. is supported by ANR ("EELS" project) and QuantERA ("MAQS" project). A.H. acknowledges financial support from PNRR MUR Project No. PE0000023-NQSTI.

[1] J. S. Bell and A. Aspect, *Speakable and Unspeakable in Quantum Mechanics: Collected Papers on Quantum Philosophy*, 2nd ed. (Cambridge University Press, Cambridge, UK, 2004).

[2] V. Scarani, *Bell Nonlocality* (Oxford University Press, Oxford, 2019).

[3] C. H. Bennett, G. Brassard, C. Crépeau, R. Jozsa, A. Peres, and W. K. Wootters, Teleporting an Unknown Quantum State via Dual Classical and Einstein-Podolsky-Rosen Channels, Phys. Rev. Lett. **70**, 1895 (1993).

[4] M. A. Nielsen and I. L. Chuang, in *Quantum Information Theory* (Cambridge University Press, Cambridge, UK, 2010), pp. 26–28.

[5] P. Shor, Algorithms for quantum computation: Discrete logarithms and factoring, in *Proceedings of the 35th Annual Symposium on Foundations of Computer Science* (IEEE, New York, 1994), pp. 124–134.

[6] L. Masanes, All Bipartite Entangled States Are Useful for Information Processing, Phys. Rev. Lett. **96**, 150501 (2006).

[7] L. Amico, R. Fazio, A. Osterloh, and V. Vedral, Entanglement in many-body systems, Rev. Mod. Phys. **80**, 517 (2008).

[8] J. Eisert, M. Cramer, and M. B. Plenio, Colloquium: Area laws for the entanglement entropy, Rev. Mod. Phys. **82**, 277 (2010).

[9] A. Hamma, S. Santra, and P. Zanardi, Quantum Entanglement in Random Physical States, Phys. Rev. Lett. **109**, 040502 (2012).

[10] A. Hamma, S. Santra, and P. Zanardi, Ensembles of physical states and random quantum circuits on graphs, Phys. Rev. A **86**, 052324 (2012).

[11] A. Osterloh, L. Amico, G. Falci, and R. Fazio, Scaling of entanglement close to a quantum phase transition, Nature (London) **416**, 608 (2002).

[12] T. J. Osborne and M. A. Nielsen, Entanglement in a simple quantum phase transition, Phys. Rev. A **66**, 032110 (2002).

[13] G. Vidal, J. I. Latorre, E. Rico, and A. Kitaev, Entanglement in Quantum Critical Phenomena, Phys. Rev. Lett. **90**, 227902 (2003).

[14] L.-A. Wu, M. S. Sarandy, and D. A. Lidar, Quantum Phase Transitions and Bipartite Entanglement, Phys. Rev. Lett. **93**, 250404 (2004).

[15] T. Roscilde, P. Verrucchi, A. Fubini, S. Haas, and V. Tognetti, Studying Quantum Spin Systems through Entanglement Estimators, Phys. Rev. Lett. **93**, 167203 (2004).

[16] M. Hofmann, A. Osterloh, and O. Gühne, Scaling of genuine multiparticle entanglement close to a quantum phase transition, Phys. Rev. B **89**, 134101 (2014).

[17] L. Amico and R. Fazio, Entanglement and magnetic order, J. Phys. A: Math. Theor. **42**, 504001 (2009).

[18] A. Hamma, R. Ionicioiu, and P. Zanardi, Ground state entanglement and geometric entropy in the kitaev model, Phys. Lett. A **337**, 22 (2005).

[19] A. Hamma, W. Zhang, S. Haas, and D. A. Lidar, Entanglement, fidelity, and topological entropy in a quantum phase transition to topological order, Phys. Rev. B **77**, 155111 (2008).

[20] A. Kitaev and J. Preskill, Topological Entanglement Entropy, Phys. Rev. Lett. **96**, 110404 (2006).

[21] X.-G. Wen, *Quantum Field Theory of Many-Body Systems: From the Origin of Sound to an Origin of Light and Electrons*, Oxford Graduate Texts (Oxford University Press, Oxford, 2007).

[22] C. Castelnovo and C. Chamon, Quantum topological phase transition at the microscopic level, Phys. Rev. B **77**, 054433 (2008).

[23] J. H. Bardarson, F. Pollmann, and J. E. Moore, Unbounded Growth of Entanglement in Models of Many-Body Localization, Phys. Rev. Lett. **109**, 017202 (2012).

[24] R. Vosk and E. Altman, Many-Body Localization in One Dimension as a Dynamical Renormalization Group Fixed Point, Phys. Rev. Lett. **110**, 067204 (2013).

[25] M. Serbyn, Z. Papić, and D. A. Abanin, Universal Slow Growth of Entanglement in Interacting Strongly Disordered Systems, Phys. Rev. Lett. **110**, 260601 (2013).

[26] M. Serbyn, Z. Papić, and D. A. Abanin, Local Conservation Laws and the Structure of the Many-Body Localized States, Phys. Rev. Lett. **111**, 127201 (2013).

[27] M. Serbyn, M. Knap, S. Gopalakrishnan, Z. Papić, N. Y. Yao, C. R. Laumann, D. A. Abanin, M. D. Lukin, and E. A. Demler, Interferometric Probes of Many-Body Localization, Phys. Rev. Lett. **113**, 147204 (2014).

[28] X. Chen, X. Yu, G. Y. Cho, B. K. Clark, and E. Fradkin, Many-body localization transition in Rokhsar-Kivelson-type wave functions, Phys. Rev. B **92**, 214204 (2015).

[29] D. A. Abanin, E. Altman, I. Bloch, and M. Serbyn, Colloquium: Many-body localization, thermalization, and entanglement, Rev. Mod. Phys. **91**, 021001 (2019).

[30] S. Szalay and Z. Kökényesi, Partial separability revisited: Necessary and sufficient criteria, Phys. Rev. A **86**, 032341 (2012).

[31] M. Walter, D. Gross, and J. Eisert, in *Multipartite Entanglement* (John Wiley and Sons, New York, 2016), Chap. 14, pp. 293–330.

[32] I. Bengtsson and K. Zyczkowski, in *Multipartite Entanglement*, 2nd ed. (Cambridge University Press, Cambridge, UK, 2017), pp. 493–543.

[33] C. Chamon, A. Hamma, and E. R. Mucciolo, Emergent Irreversibility and Entanglement Spectrum Statistics, Phys. Rev. Lett. **112**, 240501 (2014).

[34] D. Shaffer, C. Chamon, A. Hamma, and E. R. Mucciolo, Irreversibility and entanglement spectrum statistics in quantum circuits, J. Stat. Mech. (2014) P12007.

[35] D. A. Roberts and B. Yoshida, Chaos and complexity by design, J. High Energy Phys. 04 (2017) 121.

[36] P. Boykin, T. Mor, M. Pulver, V. Roychowdhury, and F. Vatan, A new universal and fault-tolerant quantum basis, Inf. Process. Lett. **75**, 101 (2000).

[37] D. Gottesman, An introduction to quantum error correction and fault-tolerant quantum computation, in *Quantum Information Science and its Contributions to Mathematics*, Proc. Sympos. Appl. Math. Vol. 68 (American Mathematical Society, Providence, RI, 2010), pp. 13–58.

[38] D. Gottesman, The Heisenberg representation of quantum computers, in *Group22: Proceedings of the XXII International Colloquium on Group Theoretical Methods in Physics*, edited by S. P. Corney, R. Delbourgo, and P. D. Jarvis (International Press, Cambridge, MA, 1999), pp. 32–43.

[39] S. Bravyi and A. Kitaev, Universal quantum computation with ideal Clifford gates and noisy ancillas, Phys. Rev. A **71**, 022316 (2005).

[40] E. Knill, Quantum computing with realistically noisy devices, Nature (London) **434**, 39 (2005).

[41] V. Veitch, S. A. H. Mousavian, D. Gottesman, and J. Emerson, The resource theory of stabilizer quantum computation, New J. Phys. **16**, 013009 (2014).

[42] M. Howard and E. Campbell, Application of a Resource Theory for Magic States to Fault-Tolerant Quantum Computing, Phys. Rev. Lett. **118**, 090501 (2017).

[43] L. Leone, S. F. E. Oliviero, and A. Hamma, Stabilizer Rényi Entropy, Phys. Rev. Lett. **128**, 050402 (2022).

[44] L. Leone, S. F. E. Oliviero, Y. Zhou, and A. Hamma, Quantum Chaos is quantum, Quantum **5**, 453 (2021).

[45] S. True and A. Hamma, Transitions in entanglement complexity in random circuits, Quantum **6**, 818 (2022).

[46] L. Leone, S. F. E. Oliviero, and A. Hamma, Isospectral twirling and quantum chaos, Entropy **23**, 1073 (2021).

[47] S. F. E. Oliviero, L. Leone, F. Caravelli, and A. Hamma, Random matrix theory of the isospectral twirling, SciPost Phys. **10**, 076 (2021).

[48] L. Leone, S. F. E. Oliviero, and A. Hamma, Nonstabilizerness determining the hardness of direct fidelity estimation, Phys. Rev. A **107**, 022429 (2023).

[49] A. Kitaev, Hidden correlations in the Hawking radiation and thermal noise, in *Talk given at the Fundamental Physics Prize Symposium* (UC Santa Barbara, CA, 2014), Vol. 10.

[50] A. W. Harrow, L. Kong, Z.-W. Liu, S. Mehraban, and P. W. Shor, Separation of out-of-time-ordered correlation and entanglement, PRX Quantum **2**, 020339 (2021).

[51] Z.-C. Yang, A. Hamma, S. M. Giampaolo, E. R. Mucciolo, and C. Chamon, Entanglement complexity in quantum many-body dynamics, thermalization, and localization, Phys. Rev. B **96**, 020408(R) (2017).

[52] Z.-W. Liu and A. Winter, Many-body quantum magic, PRX Quantum **3**, 020333 (2022).

[53] S. F. E. Oliviero, L. Leone, and A. Hamma, Magic-state resource theory for the ground state of the transverse-field Ising model, Phys. Rev. A **106**, 042426 (2022).

[54] S. F. E. Oliviero, L. Leone, A. Hamma, and S. Lloyd, Measuring magic on a quantum processor, npj Quantum Inf. **8**, 148 (2022).

[55] T. Haug and L. Piroli, Quantifying nonstabilizerness of matrix product states, Phys. Rev. B **107**, 035148 (2023).

[56] S. Zhou, Z.-C. Yang, A. Hamma, and C. Chamon, Single T gate in a Clifford circuit drives transition to universal entanglement spectrum statistics, SciPost Phys. **9**, 087 (2020).

[57] S. F. Oliviero, L. Leone, and A. Hamma, Transitions in entanglement complexity in random quantum circuits by measurements, Phys. Lett. A **418**, 127721 (2021).

[58] L. Leone, S. F. E. Oliviero, S. Piemontese, S. True, and A. Hamma, Retrieving information from a black hole using quantum machine learning, Phys. Rev. A **106**, 062434 (2022).

[59] L. Leone, S. F. E. Oliviero, S. Lloyd, and A. Hamma, Learning efficient decoders for quasi-chaotic quantum scramblers, arXiv:2212.11338.

[60] S. F. E. Oliviero, L. Leone, S. Lloyd, and A. Hamma, Black hole complexity, unscrambling, and stabilizer thermal machines, arXiv:2212.11337.

[61] G. Mahler, J. Gemmer, and M. Michel, Emergence of thermodynamic behavior within composite quantum systems, Phys. E **29**, 53 (2005).

[62] S. Popescu, A. J. Short, and A. Winter, Entanglement and the foundations of statistical mechanics, Nat. Phys. **2**, 754 (2006).

[63] S. Goldstein, J. L. Lebowitz, R. Tumulka, and N. Zanghì, Canonical Typicality, Phys. Rev. Lett. **96**, 050403 (2006).

[64] P. Reimann, Typicality for Generalized Microcanonical Ensembles, Phys. Rev. Lett. **99**, 160404 (2007).

[65] M. Rigol, V. Dunjko, and M. Olshanii, Thermalization and its mechanism for generic isolated quantum systems, Nature (London) **452**, 854 (2008).

[66] B. Derrida, Random-Energy Model: Limit of a Family of Disordered Models, Phys. Rev. Lett. **45**, 79 (1980).

[67] C. Manai and S. Warzel, Phase diagram of the quantum random energy model, J. Stat. Phys. **180**, 654 (2020).

[68] H. T. Quan, Z. Song, X. F. Liu, P. Zanardi, and C. P. Sun, Decay of Loschmidt Echo Enhanced by Quantum Criticality, Phys. Rev. Lett. **96**, 140604 (2006).

[69] P. Zanardi and N. Paunković, Ground state overlap and quantum phase transitions, Phys. Rev. E **74**, 031123 (2006).

[70] D. F. Abasto, A. Hamma, and P. Zanardi, Fidelity analysis of topological quantum phase transitions, Phys. Rev. A **78**, 010301(R) (2008).

[71] C. Castelnovo, C. Chamon, C. Mudry, and P. Pujol, From quantum mechanics to classical statistical physics: Generalized rokhsar–kivelson hamiltonians and the "stochastic matrix form" decomposition, Ann. Phys. (NY) **318**, 316 (2005).

[72] D. S. Rokhsar and S. A. Kivelson, Superconductivity and the Quantum Hard-Core Dimer Gas, Phys. Rev. Lett. **61**, 2376 (1988).

[73] T. Grover and M. P. A. Fisher, Quantum disentangled liquids, J. Stat. Mech. (2014) P10010.

[74] T. Grover and M. P. A. Fisher, Entanglement and the sign structure of quantum states, Phys. Rev. A **92**, 042308 (2015).

[75] S.-J. Gu, Fidelity approach to quantum phase transitions, Int. J. Mod. Phys. B **24**, 4371 (2010).

[76] P. Zanardi, P. Giorda, and M. Cozzini, Information-Theoretic Differential Geometry of Quantum Phase Transitions, Phys. Rev. Lett. **99**, 100603 (2007).

[77] W.-L. You, Y.-W. Li, and S.-J. Gu, Fidelity, dynamic structure factor, and susceptibility in critical phenomena, Phys. Rev. E **76**, 022101 (2007).

[78] N. T. Jacobson, S. Garnerone, S. Haas, and P. Zanardi, Scaling of the fidelity susceptibility in a disordered quantum spin chain, Phys. Rev. B **79**, 184427 (2009).

[79] H.-Q. Zhou and J. P. Barjaktarevič, Fidelity and quantum phase transitions, J. Phys. A: Math. Theor. **41**, 412001 (2008).

[80] B. Damski, Fidelity approach to quantum phase transitions in quantum Ising model, in *Quantum Criticality in Condensed Matter* (World Scientific, Singapore, 2015).

[81] P. Zanardi, M. G. A. Paris, and L. Campos Venuti, Quantum criticality as a resource for quantum estimation, Phys. Rev. A **78**, 042105 (2008).

[82] B. Derrida, The random energy model, Phys. Rep. **67**, 29 (1980).

[83] Notice that the critical temperature quoted here differs by a factor of 2 with respect to that of Ref. [66], because the variance of energy fluctuations is $\mathrm{Var}(E_\sigma) = N/2$ in that work and it is $\mathrm{Var}(E_\sigma) = N$ in this work.

[84] M. Newville, T. Stensitzki, D. B. Allen, and A. Ingargiola, *LMFIT: Non-Linear Least-Square Minimization and Curve-Fitting for Python* (Zenodo, 2014).

[85] L. Amico, F. Baroni, A. Fubini, D. Patanè, V. Tognetti, and P. Verrucchi, Divergence of the entanglement range in low-dimensional quantum systems, Phys. Rev. A **74**, 022322 (2006).

[86] B. Tomasello, D. Rossini, A. Hamma, and L. Amico, Ground-state factorization and correlations with broken symmetry, Europhys. Lett. **96**, 27002 (2011).

[87] Y. Y. Atas, E. Bogomolny, O. Giraud, and G. Roux, Distribution of the Ratio of Consecutive Level Spacings in Random Matrix Ensembles, Phys. Rev. Lett. **110**, 084101 (2013).

[88] M. L. Mehta, *Random Matrices* (Academic Press, New York, 2004).

[89] W. Tang and I. M. Khaymovich, Non-ergodic delocalized phase with Poisson level statistics, Quantum **6**, 733 (2022).

[90] V. Oganesyan and D. A. Huse, Localization of interacting fermions at high temperature, Phys. Rev. B **75**, 155111 (2007).

[91] Z.-C. Yang, C. Chamon, A. Hamma, and E. R. Mucciolo, Two-Component Structure in the Entanglement Spectrum of Highly Excited States, Phys. Rev. Lett. **115**, 267206 (2015).

[92] P. Virtanen, R. Gommers, T. E. Oliphant, M. Haberland, T. Reddy, D. Cournapeau, E. Burovski, P. Peterson, W. Weckesser *et al.*, SciPy 1.0: Fundamental algorithms for scientific computing in Python, Nat. Methods **17**, 261 (2020).

[93] H. Zhu, R. Kueng, M. Grassl, and D. Gross, The Clifford group fails gracefully to be a unitary 4-design, arXiv:1609.08172.